ULTRASTRUCTURAL AND PHYSIOLOGICAL STUDIES ON THE LONGITUDINAL BODY WALL MUSCLE OF *DOLABELLA AURICULARIA*

II. Localization of Intracellular Calcium and Its Translocation during Mechanical Activity

SUECHIKA SUZUKI and HARUO SUGI

From the Department of Physiology, School of Medicine, Teikyo University, Itabashi-ku, Tokyo 173, Japan

ABSTRACT

The localization of Ca-accumulating structures in the longitudinal body wall muscle (LBWM) of the opisthobranch mollusc *Dolabella auricularia* and their role in the contraction-relaxation cycle were studied by fixing the LBWM fibers at rest and during mechanical response to 400 mM K or to 10^{-4}–10^{-3} M acetylcholine in a 1% OsO_4 solution containing 2% K pyroantimonate. In the resting fibers, electron-opaque pyroantimonate precipitate was mostly localized at the peripheral structures, i.e., along the inner surface of the plasma membrane, at the membrane of the surface tubules, and at the sarcoplasmic reticulum. In the fibers fixed during mechanical activity, the precipitate was diffusely distributed in the myoplasm in the form of numerous particles with corresponding decrease in the amount of the precipitate at the peripheral structures. Electron-probe X-ray microanalysis showed the presence of Ca in the precipitate, indicating that the precipitate may serve as a measure of Ca localization. These results are in accord with the view that, in the LBWM, the Ca stored in the peripheral structures is released into the myoplasm to activate the contractile mechanism.

KEY WORDS molluscan smooth muscle · intracellular calcium localization · intracellular calcium translocation · electron microscopic histochemistry · pyroantimonate method · X-ray microanalysis

Although it is well established that, in vertebrate skeletal muscle, the contraction-relaxation cycle is regulated by the release of Ca from, and uptake by, the sarcoplasmic reticulum (SR) (6), the role of intracellular structures in the regulation of the contraction-relaxation cycle in various kinds of vertebrate and invertebrate smooth muscles still remains to be investigated.

In the previous paper (29), it has been shown that, in the longitudinal body wall muscle (LBWM) of an opisthobranch mollusc *Dolabella auricularia*, the contractile mechanism can be fully activated by a supramaximal concentration of K ions in the presence of Mn ions or at low pH, and by rapid cooling of the surrounding medium even after a prolonged soaking in a Ca-free solution

containing ethylene glycol-bis(β-aminoethyl ether)*N*,*N*,*N*′,*N*′-tetraacetate (EGTA). These results indicate that the LBWM fibers contain a large amount of intracellularly stored Ca which may be effectively released by a sufficient membrane depolarization or rapid cooling, so that the fibers may be fully activated in spite of the reduced Ca influx or the removal of external Ca. To obtain more definite evidence for the actual role of the intracellular structures in the LBWM, however, it seems necessary to show the localization of Ca in the intracellular structures and its translocation during mechanical activity.

Using K pyroantimonate, which is known to penetrate intact cell membrane in the presence of osmium to produce electron-opaque precipitate with intracellular cations (15, 16, 18), recent electron microscope and histochemical studies on the anterior byssal retractor muscle (ABRM) of *Mytilus edulis* (1, 27) and on the guinea pig taenia coli (28) have demonstrated that the precipitate containing Ca is released from the peripheral intracellular structures into the myoplasm during contraction. Since the pyroantimonate method also appeared to be promising for the LBWM, the present work was undertaken to study the localization of Ca in the intracellular structures in the resting LBWM fibers and the translocation of the stored Ca during mechanical activity, to obtain information about the role of the intracellular structures in the contraction-relaxation cycle of molluscan somatic smooth muscles responsible for slow locomotion and body movement.

MATERIALS AND METHODS

Electron Microscopy

The experimental methods used were identical with those previously described (29). The LBWM preparation was mounted horizontally in an experimental chamber (3 ml) filled with the experimental solution, and attached to the strain gauge to record isometric tension not only during the experiment but also during the time of fixation. At the end of each experiment, the LBWM fibers were fixed by replacing the experimental solution with a 1% OsO_4 solution (pH 6.2–6.8 by 0.01 N acetic acid) containing 2% K pyroantimonate ($K_2H_2Sb_2O_7 \cdot 4H_2O$). Fixation was terminated at 25–30 min after the application of the pyroantimonate-OsO_4 solution. The experiments were made at room temperature (18–25°C) unless otherwise stated. The fixed tissue was cut into small pieces, and rinsed with an aqueous alkaline buffer to prevent nonspecific formation of K pyroantimonate precipitate (23). Then, the pieces of tissue were dehydrated with ethanol, and embedded in Epon 812. Sections were cut on a Porter-Blum MT-1 ultramicrotome (DuPont Instruments-Sorvall, DuPont Co., Wilmington, Del.), and examined with a Hitachi HU-12AS electron microscope unstained or stained with uranyl acetate and lead acetate.

Electron Probe X-Ray Microanalysis

For histochemical identification of the precipitate of pyroantimonate salts, the sections (unstained ~2,000 Å in thickness) were mounted on a carbon-coated collodium film on copper grids, and analyzed with an energy dispersive X-ray microanalyzer (Edax 707B, Edax International Inc., Prairie View, Ill.) attached to a Hitachi HHS-2R scanning electron microscope, which was used as a scanning transmission electron microscope (STEM) with a Hitachi HH-TE2 transmission device. The STEM images (Figs. 12–15) had a higher contrast than that of the transmission electron microscope (TEM) images, though the spatial resolution was lower in the STEM images than the TEM images. The X-ray microanalysis was performed on the STEM images of the LBWM fibers in two different ways: (*a*) line-scanning analysis in which the electron beam was used as a scanning probe to record the X-ray emission from a given element (e.g., at 3,690 eV, Ca-K_α emission) along a line trace (Figs. 12 and 13); and (*b*) spot analysis in which the electron beam focused on a fixed area was used as a probe (Figs. 14 and 15). The analysis was made with an accelerating voltage of 20 kV and with a sample current of 20 nA. The X-ray emission was collected over a detecting time of 400 s unless otherwise stated.

The quantitative analysis of the precipitate was also made by use of another energy dispersive X-ray microanalyzer (Edax 707B) attached to a JEOL JEM-100C electron microscope together with a computerized EDIT system.

RESULTS

Tension Changes during the Fixation of the LBWM Fibers for Histochemical Electron Microscopy

To fix the LBWM fibers at the resting state, the preparation was soaked in the standard solution (artificial sea water) (29) containing 2 mM procaine for 5–15 min before the application of fixation solution, to minimize the mechanical response during the course of fixation. Then, the LBWM fibers were fixed, with a small tension development amounting to only <10% of the maximum K-contracture tension (Fig. 1, *a*).

The LBWM fibers were also fixed during the mechanical response to 400 mM K or to 10^{-4}–10^{-3} M acetylcholine (ACh) by applying the fixa-

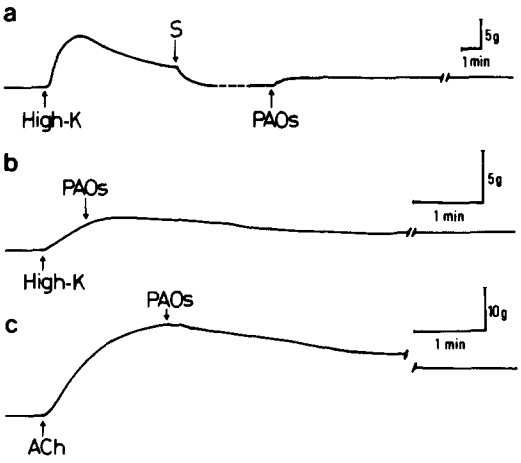

FIGURE 1 Tension changes in the LBWM fibers during the course of fixation with the pyroantimonate-OsO_4 solution. (*a*) The preparation was first made to contract with 400 mM K (*High-K*), relaxed in the standard solution containing 2 mM procaine (*S*) for 15 min, and then fixed in the pyroantimonate-OsO_4 solution (*PAOs*). Temperature, 23°C. (*b*) The preparation was made to contract with 400 mM K (*High-K*), and the pyroantimonate-OsO_4 solution (*PAOs*) was applied near the peak of contracture tension to fix the fibers in the contracted state. Temperature, 3°–6°C. (*c*) The preparation was made to contract with 10^{-3} M ACh, and the pyroantimonate-OsO_4 solution (*PAOs*) was applied at the peak of contracture tension. Temperature, 3°–6°C. In each record, the fixation was terminated after 25–30 min from the application of the fixation solution.

tion solution at or around the peak of the mechanical response (Fig. 1, *b* and *c*). Both the K- and ACh-contracture tensions tended to decrease continuously during the course of fixation. The rate of relaxation in the fixation solution could be reduced by lowering the temperature to 3°–6°C (1), so that the tension of the preparation was maintained at 50–70% of the maximum contracture tension at the completion of fixation.

Localization of Pyroantimonate Precipitate in the Resting LBWM Fibers

Figs. 2 and 3 show the transverse and the longitudinal sections of the resting LBWM fibers fixed in the pyroantimonate-OsO_4 solution, respectively. In all the fibers examined, the electron-opaque pyroantimonate precipitate was mainly localized at the peripheral part of the fibers, and also at the mitochondria, the nucleus, and the tubular element of the SR located at the central part of the fiber.

The precipitate at the peripheral part of the fiber was further examined with higher magnifications. As shown in Figs. 4 and 5, the precipitate was located along the inner surface of the plasma membrane, and at the vesicular elements of the SR near the plasma membrane, whereas little or no precipitate was observed in the extracellular space. Since the width of the electron-opaque area along the plasma membrane extends to some extent into the myoplasm, it seems possible that the precipitate is associated not only with the plasma membrane but also with other structures in its vicinity. The precipitate also appeared to be absent in the lumen of both the bottle-shaped caveolae and the surface tubules communicating with the extracellular space (29), though the precipitate was located along the inner surface of their membranes (Figs. 4 and 6). The precipitate was observed at both the inner and outer surfaces of the vesicular elements of SR subjacent to the plasma membrane (Fig. 7). The presence of a number of electron-opaque precipitates of variable size and shape in the vicinity of the plasma membrane (Figs. 4–6) may also be associated with the elements of the SR. The precipitates were abundant around the intermediate junction (Fig. 8), at which the LBWM fibers were connected with each other at their tapered ends (29), though it was not possible to show how these precipitates were associated with the elaborate tubular network present at the intermediate junction (29).

Translocation of Pyroantimonate Precipitate during Mechanical Activity

When the LBWM fiber bundles were fixed during the mechanical response to 400 mM K or 10^{-4}–10^{-3} M ACh, ~50% of the component fibers exhibited a characteristic pattern of precipitate distribution as shown in Figs. 9 and 10. In the case of both K- (Fig. 9) and ACh-contractures (Fig. 10), the electron-opaque precipitate was observed to be diffusely distributed in the myoplasm in the form of numerous particles, whereas the precipitate at the peripheral part was much less pronounced than that in the resting fibers. Closer examination of the peripheral part with higher magnifications indicated that the amount of the precipitate associated with the plasma membrane and the vesicular component of the SR

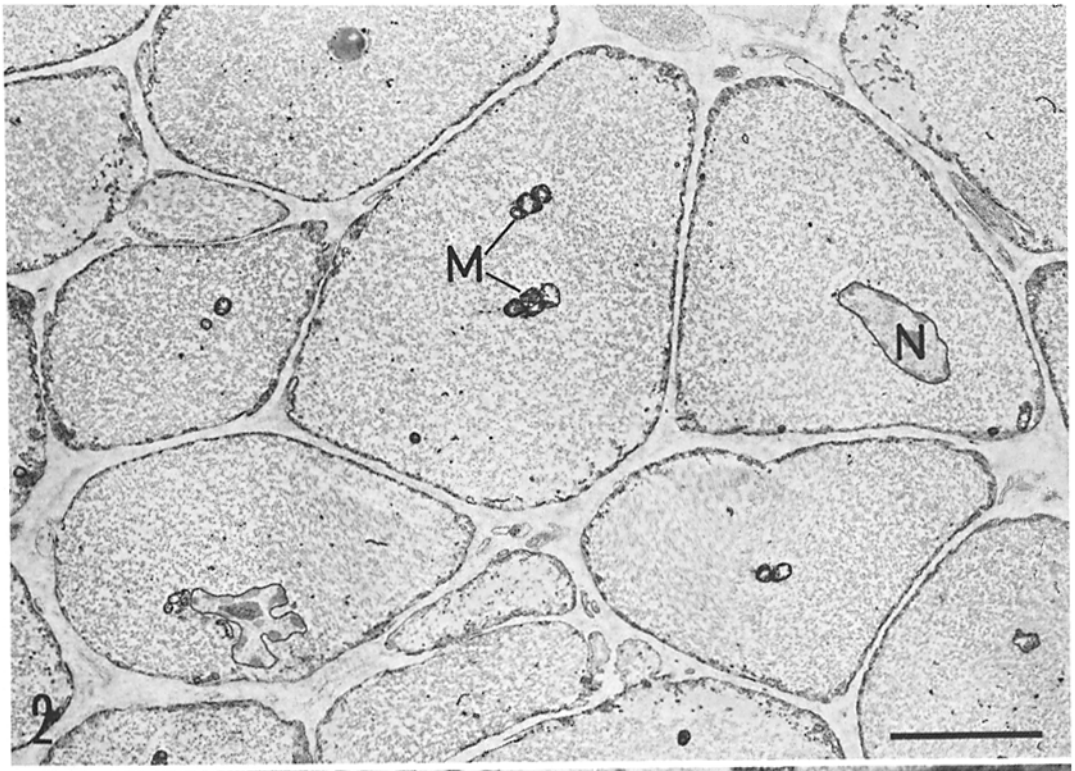

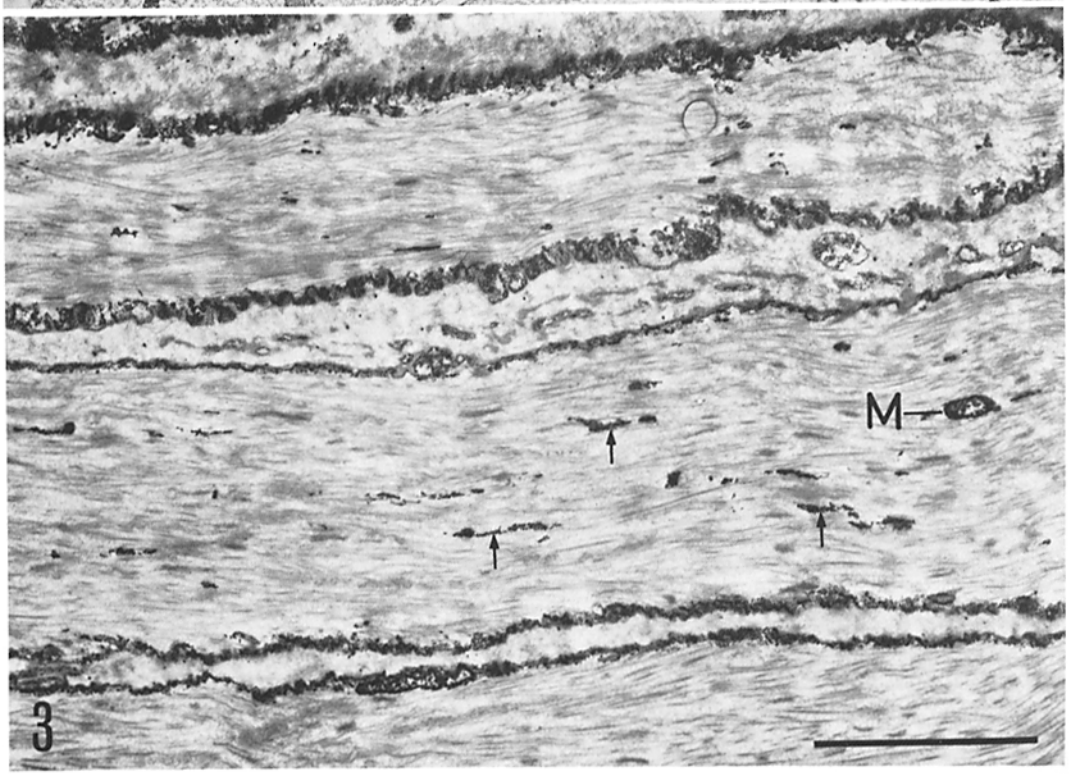

FIGURE 2 Transverse section of the resting LBWM fibers showing the localization of the electron-opaque precipitate at the peripheral part and at the mitochondria (*M*) and the nucleus (*N*). Unstained. Bar, 5 μm. × 4,000.

FIGURE 3 Longitudinal section of the resting LBWM fibers showing the localization of the precipitate at the peripheral part and at the mitochondria (*M*) and the SR (arrows) located at the central part. Double-stained (uranyl acetate and lead acetate). Bar, 5 μm. × 5,900.

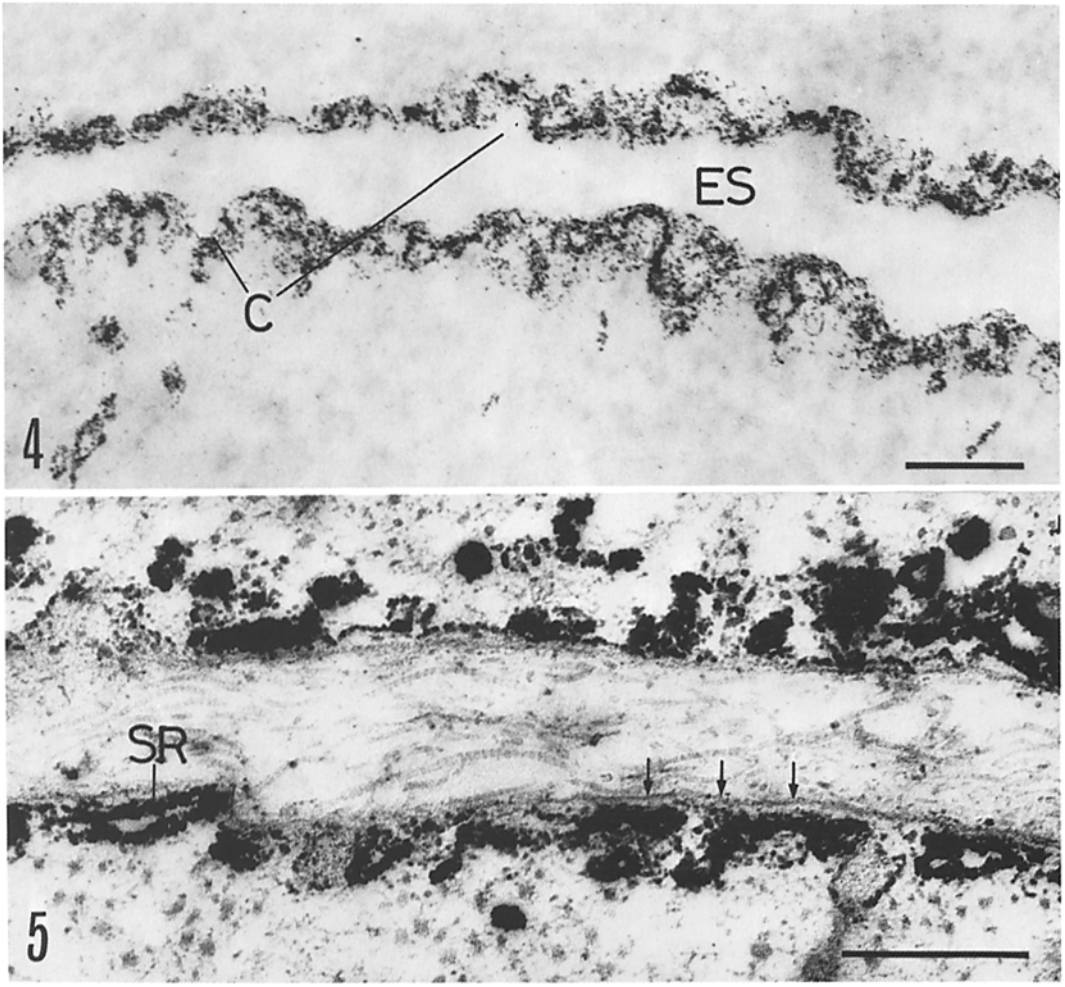

FIGURE 4 High-magnification view around the plasma membrane of the resting LBWM fibers. Unstained. Note the absence of the precipitate in the extracellular space (*ES*) and the lumen of the bottle-shaped caveolae (*C*). Bar, 0.5 μm. × 31,000.

FIGURE 5 High-magnification view around the plasma membrane of the resting LBWM fibers. Double stained. Note the localization of the precipitate along the inner surface of the plasma membrane and at the vesicular elements of the SR (*SR*). Arrows indicate the outer surface of the plasma membrane. Bar, 0.5 μm. × 49,500.

subjacent to the plasma membrane was markedly reduced (Fig. 11) as compared with the resting fibers. Since the precipitate is shown to serve as a measure of Ca localization as will be described later, the above results may be taken to indicate that the Ca localized at the peripheral structures is released into the myoplasm during mechanical activity.

The above diffuse distribution of the precipitate was observed only in ~50% of the fibers in the preparations fixed during mechanical activity, and the rest of the component fibers showed a localization of the precipitate similar to that in the resting fibers. This seems to be related to the fact that, at the completion of fixation, the tension in the LBWM fiber bundle was 50–70% of the peak contracture tension (Fig. 1, *b* and *c*); ~30–50% of the fibers might relax during the course of

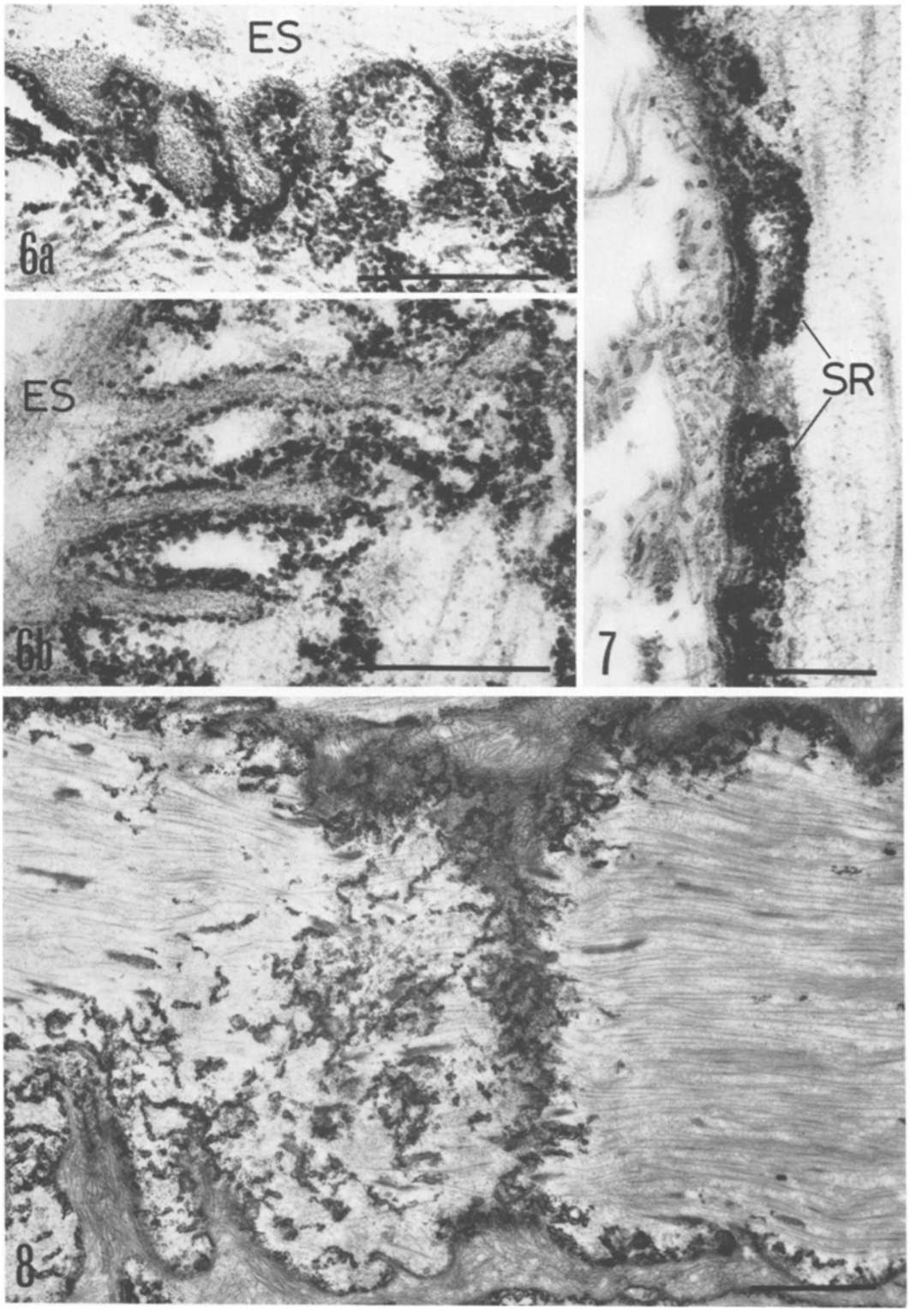
ES
6a
ES
6b
SR
7
8

fixation. Another possibility may be that not all the fibers in the LBWM are fully activated with high $[K]_0$ or ACh.

Electron Probe X-Ray Microanalysis of the Precipitate

Since pyroantimonate is known to produce an electron-opaque precipitate not only with Ca but also with other cations, the presence of Ca pyroantimonate in the precipitate in the LBWM fibers was examined by means of the electron probe X-ray microanalysis.

LINE-SCANNING ANALYSIS: Typical results of the line-scanning analysis for Ca performed on longitudinal and transverse sections of the resting fibers are shown in Figs. 12 and 13, respectively. The distribution of the X-ray emission at 3,690 eV (corresponding to the emission of Ca-K_α) along the scanning line revealed a prominent signal for Ca over the electron-opaque precipitate, whereas no significant signals for Ca were observed when the myoplasm without the precipitate was analyzed. This result indicates that the amount of Ca may be much larger in the precipitate than in the myoplasm.

SPOT ANALYSIS: Fig. 14 shows an example of the spot analysis of the precipitate in the resting fibers. The results were qualitatively the same, irrespective of the area of the precipitate on which the spot analysis was performed. The electron beam was positioned on the precipitate (point *B* in Fig. 14*a*) and also on the extracellular space where no precipitate was seen (point *A* in Fig. 14*a*) as a control. As shown in Fig. 14*b*, the X-ray spectrum of the precipitate (*dots*) always showed the most distinct peak at 3,620 eV, while that of the extracellular space (*bars*) did not. Similar results were obtained when the spot analysis was performed on the electron-opaque precipitate which was diffusely distributed in the form of particles in the myoplasm of the fibers fixed during mechanical activity (Fig. 15). When the section stained with uranyl acetate and lead acetate was used for the X-ray microanalysis, the spectrum of the precipitate also showed the most distinct peak at 3,620 eV.

Careful adjustment of the X-ray microanalyzer with the control samples (Al and Cu, Al and K pyroantimonate, and Al and $CaCl_2$) indicated that the distinct peak at 3,620 eV may result from a combination of the Sb-L_α emission (at 3,600 eV) and the Ca-K_α emission (at 3,690 eV) (Fig. 16), as has been shown by the model tests by Mizuhira (19). As a matter of fact, the X-ray spectrum of the Sb-Ca compound made by mixing equal quantities of 0.1 M $CaCl_2$ and 0.1 M K pyroantimonate solutions exhibited a distinct peak at 3,620–3,640 eV, whereas the X-ray spectrum of K pyroantimonate crystal or K pyroantimonate solution showed a spectral peak for Sb-L_α emission exactly at 3,600 eV (Fig. 17). Thus, the presence of the peak at 3,620 eV in the X-ray spectrum may be taken to indicate that the precipitate in the LBWM fibers contains Ca pyroantimonate, though the peak for Ca-K_α emission at 3,690 eV is not observable in the X-ray spectrum of the precipitate.

To obtain more direct evidence for the presence of Ca in the precipitate, quantitative analysis of the precipitate was made by means of a computerized EDIT system combined with the X-ray microanalyzer. The elemental concentration ratios relative to the concentration of Sb were computed from the data of the X-ray microanalyzer (22). In the resting fibers, the concentration ratio of Ca in the precipitate was 0.12 ± 0.02 SEM, whereas that of K was 0.35 ± 0.06 SEM. (n = 6). In the precipitate of the contracted fibers, the concentration ratio of Ca was 0.17 ± 0.03 SEM, whereas

FIGURE 6 High-magnification view of the bottle-shaped caveolae and the surface tubules in the resting LBWM fibers, showing the absence of the precipitate in their lumen communicating with the extracellular space (*ES*). Double stained. (*a*) The bottle-shaped caveolae. Bar, 0.5 μm. × 58,000. (*b*) The surface tubules. Bar, 0.5 μm. × 62,500.

FIGURE 7 High-magnification view of the vesicular elements of the SR (*SR*) subjacent to the plasma membrane in the resting LBWM fibers, showing the precipitate at both sides of their membrane. Double stained. Bar, 0.5 μm. × 46,400.

FIGURE 8 Longitudinal section of the resting LBWM fibers at the intermediate junction showing the association of the precipitate with the network of the surface tubules. Double stained. Bar, 2 μm. × 9,400.

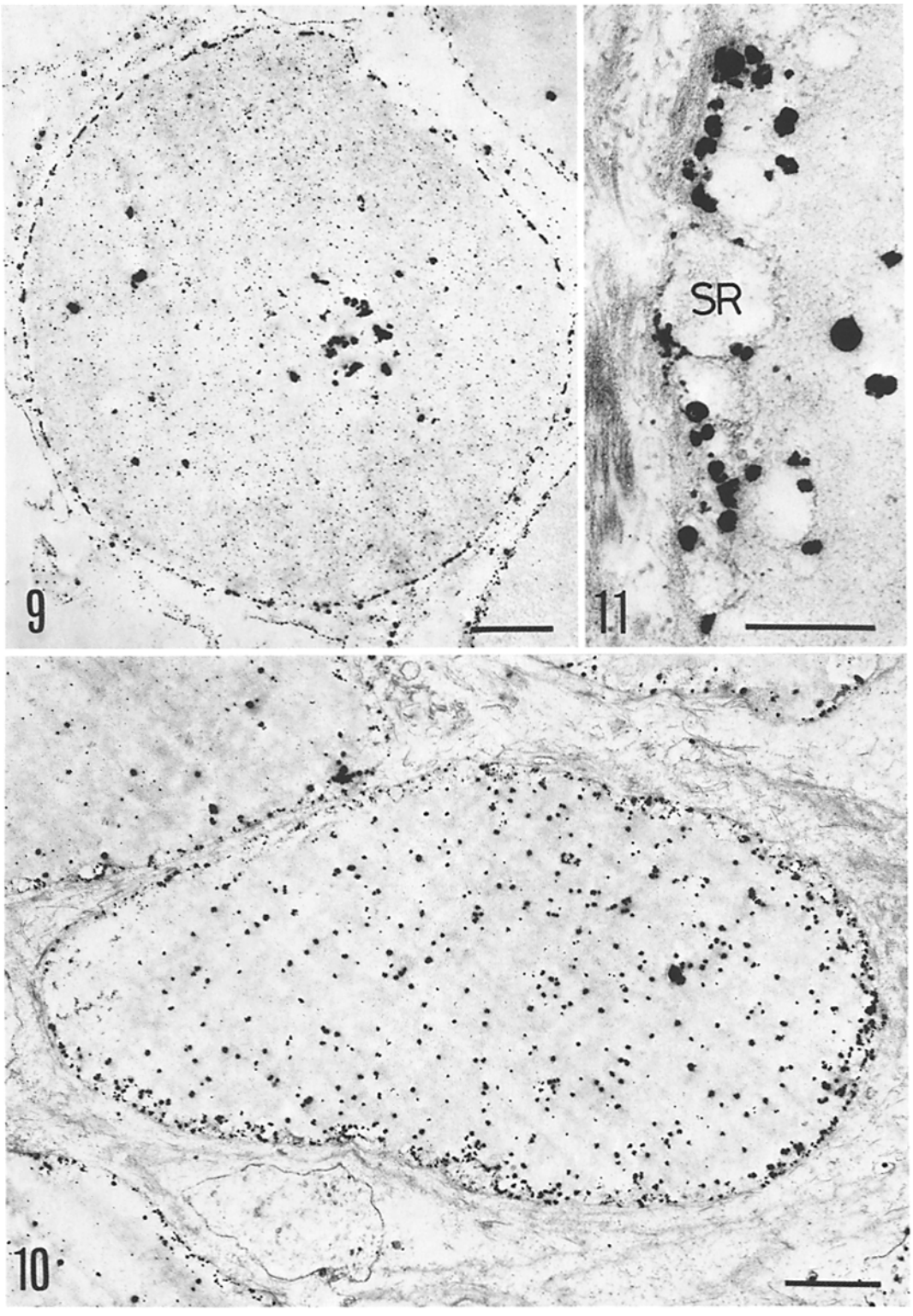
9
SR
11
10

that of K was 0.30 ± 0.04 SEM. (n = 6). Meanwhile, the presence of Na and Mg in the precipitate was not clearly detected in both cases. Thus, the above results again demonstrate the presence of Ca in the precipitate of both the resting and the contracted fibers, though its concentration ratio was smaller than that of K. Analogous results have been obtained from the quantitative analysis of the pyroantimonate precipitate in the guinea pig taenia coli (28). If it is taken into consideration that the amount of Ca ions involved in the activation of the contractile mechanism is far smaller than those of K, Na, and Mg ions in the myoplasm (6), the values of the concentration ratio of Ca in the precipitate may be taken to indicate that the precipitate serves as a measure of Ca localization.

DISCUSSION

In accordance with the finding of the preceding paper (29) that the LBWM fibers contain a large amount of intracellularly stored Ca available for the activation of the contractile mechanism, the present study has shown that, in the resting LBWM fibers, the electron-opaque pyroantimonate precipitate containing Ca is mostly localized at the peripheral structures, i.e., along the inner surface of the plasma membrane and the membrane of the surface tubules, and at the SR in close apposition to the plasma membrane or to the surface tubules. Since the contraction-relaxation cycle in intact muscle fibers is primarily controlled by the potential or permeability changes across the plasma membrane, the presence of abundant precipitate in the vicinity of the plasma membrane or of the surface tubules, consisting of tubular invaginations of the plasma membrane (29), seems to indicate the actual involvement of the peripheral structures in the release and uptake of activator Ca.

The localization of intracellular Ca at the plasma membrane and the SR has also been shown in various vertebrate smooth muscles by the use of K oxalate (13, 20, 21), ^{45}Ca (13) and K pyroantimonate (5, 7). Though the energy-dependent uptake of cations by the isolated microsomal fractions, the SR, and the mitochondria has already been demonstrated in both vertebrate (2, 4, 11, 12, 24, 25) and invertebrate (10, 26) smooth muscles, it still remains to be investigated how these intracellular structures are actually involved in the contraction-relaxation cycle in various kinds of smooth muscles.

In the present study, the pyroantimonate method, which was used successfully in the ABRM of *M. edulis* (1, 27) and in the guinea pig taenia coli (28), has proved to be useful in providing evidence for the translocation of intracellularly stored Ca during mechanical activity in the LBWM fibers of *D. auricularia*. The diffuse distribution of the electron-opaque pyroantimonate precipitate containing Ca in the form of numerous particles with corresponding decrease in the amount of the precipitate at its resting sites of localization may be completely in accord with the view that, during K- or ACh-contractures, the Ca stored in the intracellular structures is released into myoplasm to activate the myofilaments. The result that the diffuse distribution of the precipitate in the myoplasm was observed in ~50% of the fibers fixed during mechanical activity may reflect a relatively rapid rate of Ca uptake by the intracellular structures, since the contracture tension started to relax spontaneously in the contracture solutions so that the tension at the completion of fixation was 50–70% of the peak contracture tension.

Although pyroantimonate combines with Ca most rapidly under the physiological condition of cation concentrations in the myoplasm (14), it is

FIGURE 9 Transverse section of the LBWM fibers fixed during the mechanical response to 400 mM K. Note the diffuse distribution of the precipitate in the myoplasm in the form of numerous particles. Unstained. Bar, 2 μm. × 6,200.

FIGURE 10 Transverse section of the LBWM fibers fixed during the mechanical response to 10^{-3} M ACh. Note the diffuse distribution of the precipitate in the myoplasm as in Fig. 9. Stained with uranyl acetate. Bar, 2 μm. × 7,400.

FIGURE 11 High-magnification view around the plasma membrane of the fibers fixed during the mechanical response to 10^{-3} M ACh. Note that the amount of the precipitate at the vesicular elements of the SR (*SR*) is markedly reduced as compared with that shown in Fig. 7. Double stained. Bar, 0.5 μm. × 40,000.

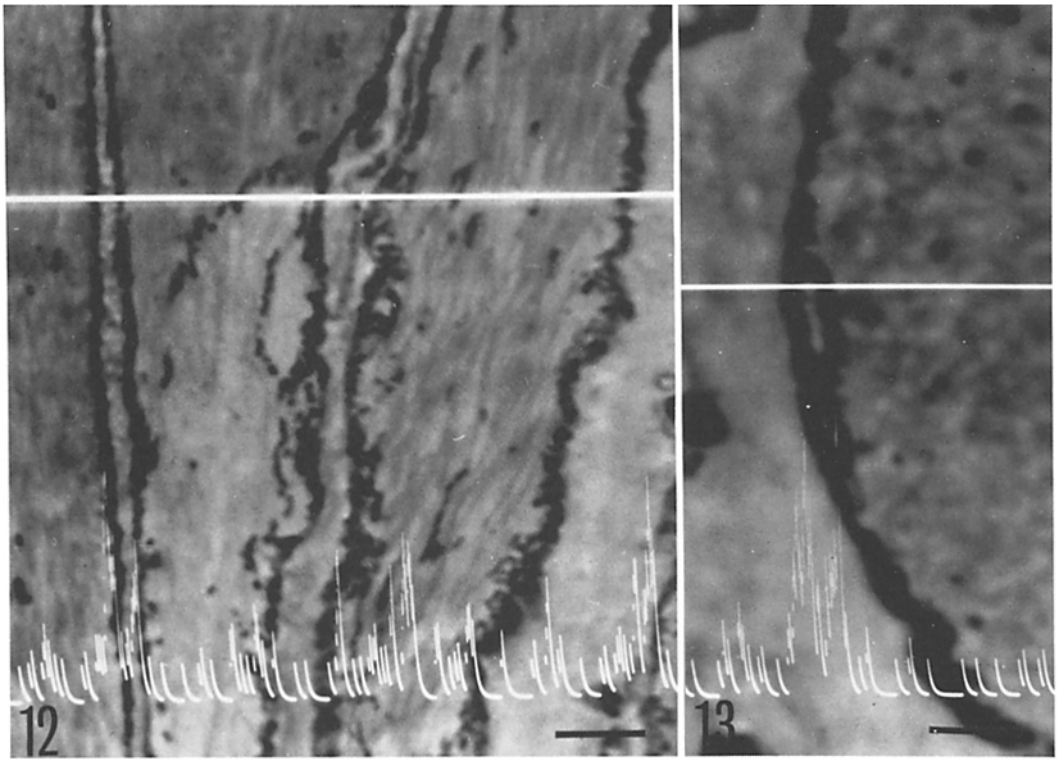

FIGURE 12 STEM image of the longitudinal section of the resting LBWM fibers showing the line-scanning analysis for Ca (Ca-K_α emission at 3,690 eV) along the scanning line (white line). Note prominent signals for Ca over the electron-opaque precipitates. Bar, 2 μm. × 5,900.

FIGURE 13 STEM image of the transverse section of the resting LBWM fibers. Note prominent signals for Ca over the precipitates as in Fig. 12. The scanning line indicated by white line is traversing the vesicular element of the SR. Bar, 1 μm. × 11,900.

FIGURE 14 Spot analysis of the electron-opaque precipitate in the resting LBWM fibers. (*a*) STEM image of the transverse section. The areas *A* and *B* were submitted to the spot analysis. Bar, 2 μm. × 8,500. (*b*) X-ray spectrum of the precipitate (*B, dots*) and that of the extracellular space (*A, bars*). The ordinate gives the number of X-ray events, and the abscissa is the individual energies of the X ray in KeV (20 eV/CH). Note the most distant peak at 3,620 eV in the X-ray spectrum of the precipitate. Vertical white line indicates the position of Sb-L_α emission at 3,600 eV.

FIGURE 15 Spot analysis of the electron-opaque precipitate diffusely distributed in the form of numerous particles in the myoplasm of the contracted LBWM fibers. (*a*) STEM image of the fibers fixed during the mechanical response to 10^{-3} M ACh. The areas *A* and *B* were submitted to the spot analysis. Bar, 2 μm. × 8,300. (*b*) X-ray spectrum of the precipitate (*B, dots*) and that of the extracellular space (*A, bars*). The abscissa gives the individual energies of the X ray in KeV (20 eV/CH). Note the most distinct spectral peak at 3,620 eV. Vertical white line indicates 3,600 eV as in Fig. 14*b*.

FIGURE 16 X-ray spectrum of the precipitate (*bars*) in the resting LBWM fibers and that of the standard K pyroantimonate (*dots*) used for the adjustment of the microanalyzer. The abscissa gives the individual energies of the X ray in KeV (10 eV/CH). Note the most distinct peak at 3,620 eV in the X-ray spectrum of the precipitate. Vertical white line indicates the position of Sb-L_α emission at 3,600 eV. X-ray emission was collected for 400 s (*dot-spectrum*) and for 47 s (*bar-spectrum*).

FIGURE 17 X-ray spectrum of the Sb-Ca compound prepared by mixing equal quantities of $CaCl_2$ and K pyroantimonate solution (*dots*) and that of K pyroantimonate crystal (*bars*). The abscissa gives the individual energies of the X ray in KeV (20 eV/CH). Note the most distinct peak at 3,640 eV in the X-ray spectrum of the Sb-Ca compound. Vertical white line indicates 3,600 eV. In both spectra, X-ray emission was collected for 80 s.

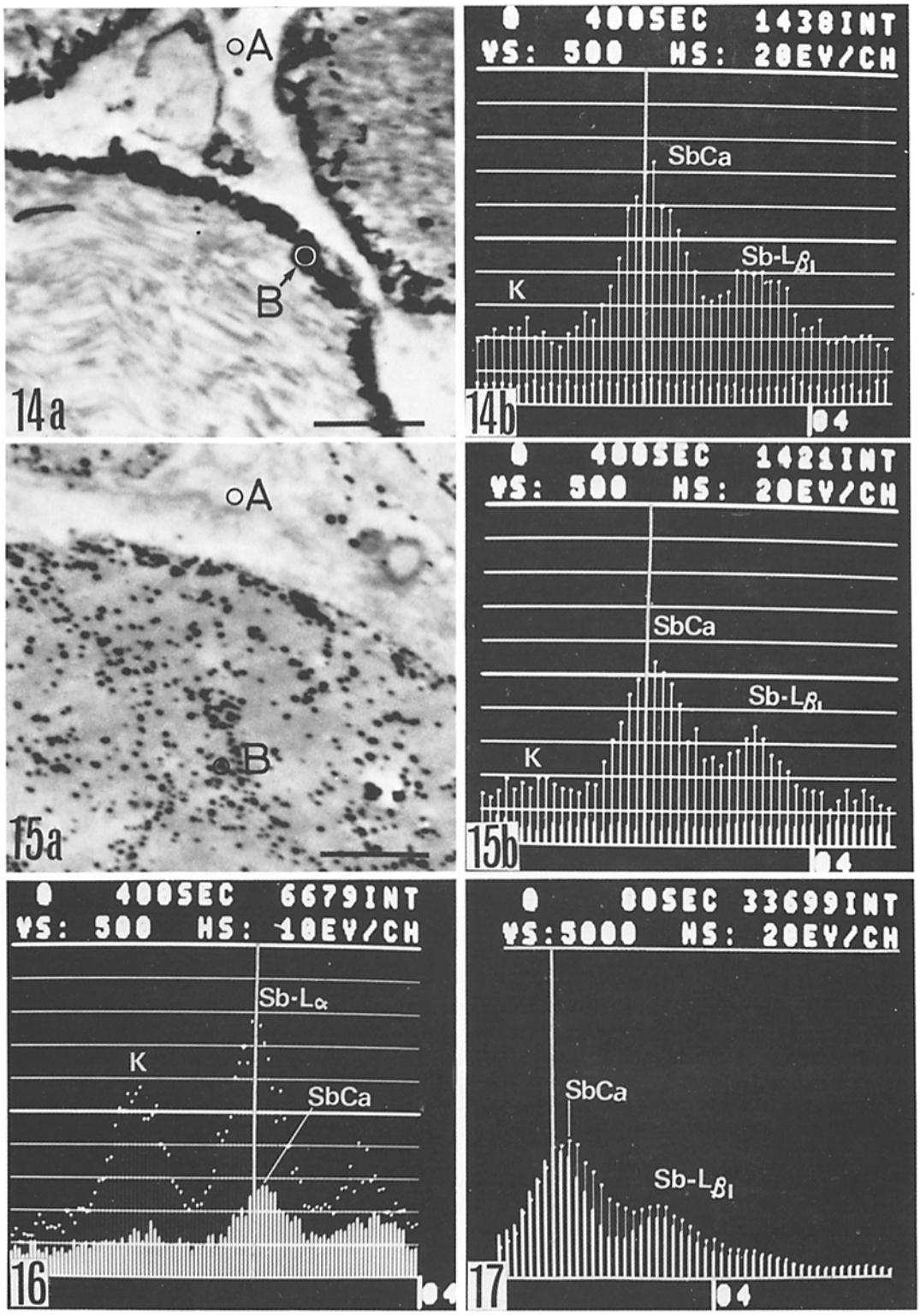
A
B
14a
400SEC 1438INT
VS: 500 HS: 20EV/CH
SbCa
Sb-Lβ1
K
14b
A
B
15a
400SEC 1421INT
VS: 500 HS: 20EV/CH
SbCa
Sb-Lβ1
K
15b
400SEC 6679INT
VS: 500 HS: 10EV/CH
Sb-Lα
K
SbCa
16
00SEC 33699INT
VS:5000 HS: 20EV/CH
SbCa
Sb-Lβ1
17

also known to readily combine with Na, and is used as an indicator for intracellular Na localization (3, 8, 15, 16, 17, 23). Moreover, pyroantimonate combines with K to form the precipitate in ethanol (9). In the present study, the presence of K in the precipitate was also noticed by the peak for the K-K_α emission at 3,310 eV, whereas the peaks for Na and Mg were not clearly observable in the X-ray spectrum of the precipitate. The presence of K in the precipitate was further confirmed by the quantitative analysis with the EDIT system. These results indicate that the electron-opaque precipitate also contains K pyroantimonate which may be formed mostly during the dehydration of the tissues with ethanol. The translocation of the precipitate in the LBWM fibers fixed during mechanical activity, however, may not be readily explained without assuming the release of Ca from the intracellular structures into the myoplasm. It may be that, when the contracted fibers are immersed in the pyroantimonate-OsO_4 solution, the Ca ions released into the myoplasm combine with pyroantimonate to form numerous deposits distributed in the myoplasm, and in the subsequent treatment of the tissues with ethanol K pyroantimonate precipitates around the deposits of Ca pyroantimonate already present. If this interpretation is correct, the translocation of the precipitate would reflect the physiological role of the intracellularly stored Ca, and the additional formation of K pyroantimonate precipitate would simply increase the amount of the precipitate but not alter its localization. Model tests to confirm whether this is actually the case are desired to establish the pyroantimonate method as an effective means of studying the Ca translocation during the physiological muscle contraction.

The authors wish to thank Dr. J. C. Russ and Dr. T. Daimon for their helpful suggestions and discussions concerning the electron probe X-ray microanalysis of the precipitate, and the staff of the Electron Optic Division, JEOL Ltd. for providing facilities to use the microanalyzer with the EDIT system.

Received for publication 2 August 1977, and in revised form 20 April 1978.

REFERENCES

1. Atsumi, S., and H. Sugi. 1976. Localization of calcium-accumulating structures in the anterior byssal retractor muscle of *Mytilus edulis* and their role in the regulation of active and catch contraction. *J. Physiol. (Lond.).* **257**:549–560.
2. Batra, S. C., and E. E. Daniel. 1971. ATP-dependent Ca uptake by subcellular fractions of uterine smooth muscle. *Comp. Biochem. Physiol. A. Comp. Physiol.* **38**:369–385.
3. Bulger, R. E. 1969. Use of potassium pyroantimonate in the localization of sodium ions in rat kidney tissue. *J. Cell Biol.* **40**:79–94.
4. Carsten, M. E. 1969. Role of calcium binding by sarcoplasmic reticulum in the contraction and relaxation of uterine smooth muscle. *J. Gen. Physiol.* **53**:414–426.
5. Debbas, G., L. Hoffman, E. J. Landon, and L. Hurwitz. 1975. Electron microscopic localization of calcium in vascular smooth muscle. *Anat. Rec.* **182**:447–472.
6. Ebashi, S., and M. Endo. 1968. Calcium ion and muscle contraction. *Prog. Biophys. Mol. Biol.* **18**:123–183.
7. Goodford, P. J., and M. W. Wolowyk. 1972. Localization of cation interactions in the smooth muscle of the guinea-pig taenia coli. *J. Physiol. (Lond.).* **224**:521–535.
8. Hardin, J. H., and S. S. Spicer. 1970. Ultrastructure of nucleoli of rat trigeminal ganglia: comparison of routine with pyroantimonate-osmium tetroxide fixation. *J. Ultrastruct. Res.* **31**:16–36.
9. Hayat, M. A. 1975. Positive Staining for Electron Microscopy. Van Nostrand Reinhold Co., New York.
10. Heumann, H.-G. 1969. Calciumakkumulierende Strukturen in einem glatten Wirbellosenmuskel. *Protoplasma.* **67**:111–115.
11. Heumann, H.-G. 1976. The subcellular localization of calcium in vertebrate smooth muscle. Calcium-containing and calcium accumulating structures in muscle cells of mouse intestine. *Cell Tissue Res.* **169**:221–231.
12. Hurwitz, L., D. F. Fitzpatrick, G. Debbas, and E. J. Landon. 1973. Localization of calcium pump activity in smooth muscle. *Science (Wash. D. C.).* **179**:384–386.
13. Jonas, L., and U. Zelck. 1974. The subcellular calcium distribution in the smooth muscle cells of the pig coronary artery. *Exp. Cell Res.* **89**:352–358.
14. Klein, R. L., S.-S. Yen, and Å. Thureson-Klein. 1972. Critique on the K-pyroantimonate method for semiquantitative estimation of cations in conjunction with electron microscopy. *J. Histochem. Cytochem.* **20**:65–78.
15. Komnick, H. 1962. Electronenmikroskopische Lokalisation von Na^+ and Cl^- in zellen und geweben. *Protoplasma.* **55**:414–418.
16. Komnick, H., and U. Komnick. 1963. Electronenmikroskopische Untersuchungen zur funktionellen Morphologie des Ionentransportes in der Sarzdrüse von *Larus argentatus*. *Z. Zellforsch. Mikrosk. Anat.* **60**:163–203.
17. Lane, B. P., and E. Martin. 1969. Electron probe analysis of cationic species in pyroantimonate precipitates in epon-embedded tissue. *J. Histochem. Cytochem.* **17**:102–106.
18. Legato, M. J., and G. A. Langer. 1969. The subcellular localization of calcium ion in mammalian myocardium. *J. Cell Biol.* **41**:401–423.
19. Mizuhira, V. 1976. Elemental analysis of biological specimens by electron probe X-ray microanalysis. *Acta Histochem. Cytochem.* **9**:69–87.
20. Popescu, L. M., and I. Diculescu. 1975. Calcium in smooth muscle sarcoplasmic reticulum *in situ*. Conventional and X-ray analytical electron microscopy. *J. Cell Biol.* **67**:911–918.
21. Popescu, L. M., I. Diculescu, U. Zelck, and N. Ionescu. 1974. Ultrastructural distribution of calcium in smooth muscle cells and quantitative study. *Cell Tissue Res.* **154**:357–378.
22. Russ, J. C. 1974. The direct element ratio model for quantitative analysis of thin sections. *In* Microprobe Analysis as Applied to Cells and Tissues. T. Hall, P. Echlein and R. Kaufmann, editors. Academic Press, Inc., New York. 269–276.
23. Shiina, S.-I., V. Mizuhira, T. Amakawa, and Y. Futaesaku. 1970. An analysis of the histochemical procedure for sodium ion detection. *J. Histochem. Cytochem.* **18**:644–649.
24. Somlyo, A. P., A. V. Somlyo, C. E. Devine, P. D. Peters, and T. A. Hall. 1974. Electron microscopy and electron probe analysis of mitochondrial cation accumulation in smooth muscle. *J. Cell Biol.* **61**:723–742.
25. Somlyo, A. V., and A. P. Somlyo. 1971. Strontium accumulation by sarcoplasmic reticulum and mitochondria in vascular smooth muscle. *Science (Wash. D. C.).* **174**:955–958.
26. Stössel, W., and E. Zebe. 1968. Zur intrazellulären Regulation der Kontraktionsaktivität. *Pflügers Arch. Ges. Physiol. Menschen Tiere.* **302**:38–56.
27. Sugi, H., and S. Atsumi. 1973. Localization of calcium-accumulating structures in the anterior byssal retractor muscle of *Mytilus edulis* and their role in excitation-contraction coupling. *Proc. Jpn. Acad.* **49**:638–642.
28. Sugi, H., and T. Daimon. 1977. Translocation of intracellularly stored calcium during the contraction-relaxation cycle in guinea-pig taenia coli. *Nature (Lond.).* **269**:436–438.
29. Sugi, H., and S. Suzuki. 1978. Ultrastructural and physiological studies on the longitudinal body wall muscle of *Dolabella auricularia*. I. Mechanical response and ultrastructure. *J. Cell Biol.* **79**:454–466.